RSC Advances

ROYAL SOCIETY
OF CHEMISTRY

www.rsc.org/advances
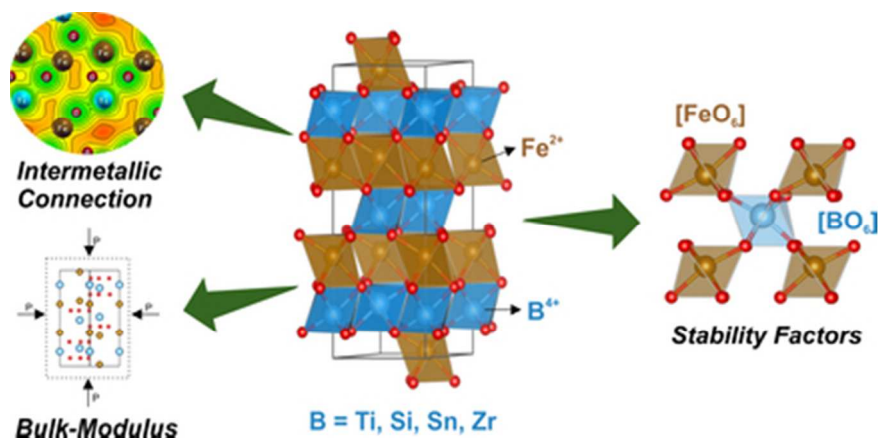
36x17mm (300 x 300 DPI)

Journal Name

RSCPublishing

ARTICLE

Structural, Electronic and Elastic properties of FeBO$_3$ (B = Ti, Sn, Si, Zr) Ilmenite: A Density Functional Theory Study

R. A. P. Ribeiro and S. R. de Lázaro[a]

FeBO$_3$ (B = Ti, Sn, Si, Zr) materials were simulated from Density Functional Theory (DFT) at B3LYP hybrid functional to investigate the B-site replacement effect on the ilmenite structure. Lattice Parameters, Bond Distances, Bulk-Modulus, Density of States (DOS), Mulliken Population Analysis and Charge Density Maps were examined. Calculated structural parameters were in agreement with experimental results and revealed that the unit cell volume was controlled by the ionic radius of B-site metals. The Bulk-Modulus obtained indicated that these results were influenced by different material density. Electronic results showed that Band-Gap and structural stability were influenced by the energy levels and electronegativity of metals occupying the B-site, as shown in the literature. Mulliken Population Analysis and Charge Density maps show the magnetic property for Fe atom in d^6 configuration and charge corridor formation in [001] direction due to the intermetallic connection.

1. Introduction

Iron Titanate (FeTiO$_3$) is a very common mineral on the earth surface which in recent years has attracted high technological interest due to its potential applications in spintronic, electronic and opto-electronic devices, high temperature integrated circuits, photocatalysis, and others.[1-5] The crystal structure of this material is similar to the Corundum (Al$_2$O$_3$) having a trigonal symmetry with *R-3* (n° 148) space group, where the anions are densely packed in a hexagonal array with cations occupying two-thirds of the possible octahedral sites in an alternating arrangement enabling the sharing of the octahedron AO$_6$ edges.[6, 7] This material can also take the structure of other polymorphs (LiNbO$_3$, Perovskite) depending on the pressure conditions. Furthermore, the cations structural distribution enables charge transfer between the octahedral altering the valence states of the metals (Fe^{2+}Ti^{4+} ↔ Fe^{3+}Ti^{3+}) under extreme pressure conditions.[8-11] Recently, Varga and co-workers[12] have shown experimentally that the mineral Ilmenite is a multiferroic material when stabilized in LiNbO$_3$ phase (*R3c*), confirming the first-principles predictions.[13] This discovery increases the interest in the search of multiferroic materials based on ilmenite structure.

Several other mixed oxides with general formula ABO$_3$ adopt the ilmenite structure, such as ZnSnO$_3$, CdSnO$_3$, FeGeO$_3$, MgSiO$_3$, MnTiO$_3$, MnSnO$_3$ with important technological applications in the development of solar cells, umpteen sensors, magnetic materials, and others.[14-17] Furthermore, experimental evidence suggests that a number of these oxides can be converted into the ferroelectric *R3c* structure through high-pressure route.[18] For instance, ZnSnO$_3$[19, 20], MnSnO$_3$ and MnTiO$_3$[21] materials which were synthesized under such conditions could be used for ferroelectric applications due to their large polarization. However, few studies report the synthesis and properties of ilmenite structure for Fe-based

materials with Zr^{4+}, Si^{4+} and Sn^{4+} cations. FeSiO$_3$ has been reported only as orthoferrosilite in the perovskite structure[22] or as an end-member of (Fe,Mg)SiO$_3$-akimotoite[23] mineral. Iron stannate was investigated from theoretical calculations by Zhu and co-workers[24] in the ilmenite structure and predicted as unstable under thermodynamic equilibrium conditions. Regarding iron zirconate there are no reports about ilmenite structure, but this cation (Zr^{4+}) has some interesting properties for perovskite materials.[25]

In recent years, many theoretical and experimental studies have been proposed to discuss the structural and electronic properties of other classes of materials. These studies show high scientific and technological importance as regards the design of new materials and the discovery of new properties. Litmein and co-workers[26] investigating the structure of RXRh$_3$ (X = Sc, Y, La and Lu) perovskites have shown that the change of the B-cation provides structural, electronic and elastic changes in the crystal structure as a function of the size and electronic distribution of elements. Similarly, Belik and Yi[27] reviewing the crystal chemistry of perovskites with small A-cations observed that magnetic and multiferroic behaviour is dependent on structural distortions caused by A-site cations. Similar studies have been performed with several types of materials, from simple oxides, such as, CdX (X = S, Se, Te), selenides (M$_2$Se) and carbides (MC, M= Ti, V, Zr, Li, Na, Rb), to complex perovskites as Pb$_2$CrMO$_6$ (M = Mo, W, Re) and Ba$_2$MWO$_6$ (M = Mg, Ni, Zn).[28-32]

First-principles calculations continue to play an important role in the materials design for future technologies. Density Functional Theory (DFT) is the most successful approach used in these calculations due to the treatment of complex electron-electron interactions.[33] To describe these kinetic and energetic interactions it is necessary to use approximate functionals. The simplest approximations used in DFT are Local Density Approximations (LDA) and Generalized Gradient

RSC Advances Accepted Manuscript

Approximation (GGA), but especially on solid state calculations such functionals fail in the band-gap and magnetic moments measurement due to strong Coulomb repulsion.[34, 35] The most promising functionals for solid state calculations are characterized by a mixing of non-local Hartree-Fock (HF) approach with a DFT exchange, denominated hybrid functionals. A large number of hybrid functionals are described in the literature, such as B3PW, PBE0, B3LYP, HSE, meta hybrid GGA and others. Such functionals are enormously successful in quantum chemistry calculations for different applications.[35, 36] Theoretical results suggested that the B3LYP, used in this work, is the best choice among the hybrid functionals for produces ground state energy surfaces and significantly improves energy gaps, as well as to predict the magnetic coupling constants for a variety of materials.[34, 37]

In the present work, the structural, electronic and elastic properties for the $FeBO_3$ (B = Ti, Sn, Si, Zr) materials in ilmenite structure were investigated from Density Functional Theory (DFT) using B3LYP hybrid functional. The aim of this manuscript is to provide a more detailed description of the ilmenite structural properties as a function of molecular composition.

2. Theoretical Section

Iron titanate ($FeTiO_3$) is found naturally in trigonal symmetry of the ilmenite structure, *R-3* spatial group (n° 148) and lattice parameters a = b = 5.0875 Å and c = 14.0827 Å. The atomic spatial arrangement is defined by internal coordinates: Fe (0, 0, 0.3536), Ti (0, 0, 0.1446) and (0.3172, 0.0234, 0.2450).[38] The crystalline structure of $FeTiO_3$ material is shown in Figure 1. Other models were produced from this crystalline structure performing the replacement of Ti atom by Sn, Zr and Si atoms. As preliminary step, the unit cell for all models ($FeBO_3$, B=Ti, Sn, Si, Zr) was fully relaxed in relation to the system total energy.

[Insert Figure 1]

In this work, all simulations were based on the Density Functional Theory (DFT) using hybrid functional consisting of a non-local exchange functional developed by Becke[39, 40] combined with a correlation functional based on gradient of electronic density (GGA) developed by Lee, Yang and Parr.[41] The simulations were performed using the CRYSTAL09 package.[42] Fe, Ti, Si, Zr and O atoms were described from atomic basis sets composed of Gaussian type functions with Triple-Zeta polarization (TZVP) developed by Peintinger and co-workers.[43] However, to describe the Sn atom an atomic basis set of pseudopotential type was used (Sn_DURAND-21G*)[44], where the core electrons are described by an effective potential defined by Durand and Barthelat.[45]

The lattice parameters were optimized in relation to the system total energy using mono and bielectronic integrals converged with pre-defined criteria of 10^{-8} Hartree. The diagonalization of the matrix density was carried out using the grid of *k* points in reciprocal space according to the Monkhorst-Pack method.[46] The shrink factor was set to 6 x 6 (Gilat Web) corresponding to 40 independent *k* points in the Brillouin zone. It was preliminary found that the energy difference between ferromagnetic and antiferromagnetic states was very small and, therefore, the ferromagnetic model was used.[47] Electronic properties, such as, Density of States (DOS), Mulliken Population Analysis and Charge Density Maps were obtained from unit cell optimized. For the elastic property evaluation Bulk-Modulus (B_0) concept calculated from Energy vs Volume (V) theoretical curve was used. The CRYSTAL09

program can perform an automated scan over the volume in order to compute energy (E) versus volume (V) curves, from a full V-constrained geometry optimization for each V. These results are then fitted to third-order isothermal Birch-Murnaghan's equation to calculate equilibrium properties such as bulk modulus (B_0), its first derivative (B_0') with respect to the pressure and volume/pressure dependence on the energy, enthalpy and bulk modulus.[48]

3. Results and Discussion

Structural Parameters

Structural modifications on crystalline systems are available from lattice parameters to observed expansion or unit cell compression. In general, such modifications represent the new equilibrium between repulsive and attractive forces inside solids generating a new distribution of the electronic density and new properties. Experimentally, these properties are widely researched and very important in crystalline nanostructures, mainly, ferroelectric and ferromagnetic properties due to their application into electronic industry. In particular, magnetic properties have been deeply researched because of the development of spintronic. This new technology is promising for the optimization of the calculation capacity into computers. Theoretical results for lattice parameters of the $FeBO_3$ (B = Ti, Si, Sn, Zr) materials are shown in Table 1. Structural parameters calculated for $FeTiO_3$ material showed good agreement with experimental results and similar deviations to other DFT theoretical studies.[49] In particular, it was observed that lattice parameters were modified directly from bond distances of the atoms localized in the ilmenite structure B site. For instance, Si-O bond distance was found as low bond length and, consequently, the $FeSiO_3$ material has contracted lattice parameters. Such structural distortions are discussed as responsible for the origin of ferroelectric, optical and magnetic properties, because local disorders were created inside the crystalline structure.[50-52] For all models, the Fe-O_{ax}, Fe-O_{eq}, B-O_{ax} and B-O_{eq} bond distances (Fig. 1, Table 1) were not equal showing that FeO_6 and BO_6 clusters were distorted, consequently, changing the local charge density shared among atoms of the crystalline structure. These effects will be discussed in the Electronic Properties Section.

Table 1 Theoretical and experimental results for lattice parameters (in Å) of $FeBO_3$ (B = Ti, Si, Sn, Zr) materials. M-Oax and M-Oeq correspond to axial and equatorial bonds (in Å) for BO_6 and FeO_6 clusters, respectively.

Models	Lattice Parameters		Bond Distances M-O			
	a	c	Fe-$O_{ax.}$	Fe-$O_{eq.}$	B-$O_{ax.}$	B-$O_{eq.}$
$FeTiO_3$	5.093	14.226	2.180	2.100	2.120	1.860
$FeSiO_3$	4.762	14.191	2.237	2.065	1.842	1.769
$FeSnO_3$	5.275	14.437	2.263	2.115	2.093	2.017
$FeZrO_3$	5.453	14.242	2.216	2.152	2.223	2.057
Exp.*	5.087	14.083	2.200	2.080	2.090	1.870

*Experimental results for $FeTiO_3$ are taken from Ref.[34]

Elastic Properties

Bulk-modulus is defined as the resistance of a substance against a uniform external pressure and it can be calculated from theoretical EOS curves using Birch-Murnaghan equation of state[53], as previously explained in Section 2. Another point of view about bulk-modulus is related to thermodynamically stability of solids from elastic constants concept to deform

crystalline structures. However, the elastic constants must satisfy thermodynamic stability limits corresponding to the physical requirement that the elastic strain energy be definite positive because negative values do not represent physical requirement.[54] Nevertheless, this interpretation is based on a strain physical model, which only considers thermodynamic states required for the crystalline structure of interest. Therefore, we show below that it is possible to understand the negative value for bulk-modulus as a mechanical stability criterion only when compared to the same crystalline structure. This interpretation is only possible due to the fundamental concept of solid mechanics deformation, which is intrinsically associated to the solid chemical nature through attractive and repulsive forces. Thereby, the change of cations in the same crystalline structure modifies proportionality the equilibrium between attractive and repulsive forces of solid through chemical bond.

Thus, the $FeBO_3$ (B = Ti, Si, Sn, Zr) materials elastic property is shown in Figure 2. From these results the equilibrium volumes for $FeTiO_3$, $FeSiO_3$, $FeSnO_3$ and $FeZrO_3$ structures were calculated as 321.77 Å^3, 279.98 Å^3, 352.73 Å^3 and 369.14 Å^3, respectively.

[Insert Figure 2]

The bulk-modulus calculated for $FeBO_3$ (B = Ti, Si, Sn and Zr) materials is shown in Table 2. These theoretical results revealed that $FeTiO_3$ bulk-modulus was in agreement with the experimental and another theoretical result[49]. Furthermore, it was possible to determine that the bulk-modulus decreased in order $FeTiO_3 > FeSiO_3 > FeZrO_3 > FeSnO_3$. Bulk-modulus is a thermodynamic quantity, which changes in relation to relative density (ρ). In general, the order shown before indicates the bulk-modulus decreases when ρ is increased. An exception is $FeSiO_3$ material, which shows bulk-modulus smaller than the $FeTiO_3$ material even with lower density. Such deviation may be related to the smaller Si-O bond distance and the fact that the Si atom is hybridized under coordination number 6. This Si atom hybridization state is not ordinary making the SiO_6 cluster a tensioned molecular structure favouring a phase transition or decomposition to simple oxides. The negative bulk-modulus result is considered a factor of thermodynamic instability regarding the mechanical deformation[55, 56], as previously discussed. Thus, the $FeSnO_3$ material exhibited instability under theoretical equilibrium condition (P = 0 atm and T = 0 K) and the difficulty of synthesis by conventional methods. This result was in accordance with the theoretical phase diagram obtained by Zhu and co-workers.[24] However, as well as $ZnSnO_3$,[19, 20] the high-temperature, high-pressure and thin film growth techniques may be useful for the synthesis of this material in the ilmenite structure. At the same time, bulk-modulus for $FeSiO_3$ and $FeZrO_3$ suggest that these materials were stable in the ilmenite structure for theoretical equilibrium conditions.

Table 2 Theoretical and experimental results for Bulk-Modulus (in GPa) and theoretical results for Relative Density (ρ in g.cm^{-3}) of the $FeBO_3$ (B = Ti, Si, Sn, Zr) materials.

| Models | Bulk-Modulus | | | ρ |
	This Work	Theoretical[49]	Exp.[38]	Theoretical
$FeTiO_3$	183.24	172	177	4.733
$FeSiO_3$	43.70	-	-	4.716
$FeZrO_3$	12.38	-	-	5.266
$FeSnO_3$	-731.76	-	-	6.410

Electronic Properties

[Insert Figure 3]

Electronic Properties for the $FeBO_3$ (B = Ti, Si, Sn, Zr) materials were investigated from theoretical results for Density of States (DOS), Mulliken Population Analysis and Charge Density Maps. From the total calculated and atom-resolved DOS (Fig. 3) for $FeBO_3$ (B = Ti, Si, Sn, Zr) structure, it was observed that for all models the Valence Band (VB) was predominantly composed of O (2p) and Fe (3d, 4s, 4p) atomic states. Whereas, Fe (3d, 4s, 4p) and Ti (3d, 4s, 4p) and Si (3s, 3p, 3d) and Sn (5s, 5p) and Zr (4d, 5s, 5p) atomic states contributed predominantly for the Conduction Band (CB). In particular, the contribution observed for Sn atoms is featured from pseudopotential atomic basis set as discussed for $CdSnO_3$ in ilmenite and perovskite structures.[57, 58] The influence of B = Ti, Si, Sn and Zr cation in the ilmenite structure is shown from the CB energetic displacement. The energy range displaced for CB shows more degenerated electronic levels in crescent order: $FeTiO_3 < FeSiO_3 = FeSnO_3 < FeZrO_3$; such fact has as consequence more specific energy levels, mainly, to locate spin states.

In the $FeTiO_3$ model, the Fe-O bonding interactions were located between -4 and -7 eV and the band-Gap was calculated as 2.51 eV, in agreement with experimental results (2.5-2.9 eV).[5, 59, 60] For $FeSiO_3$ and $FeSnO_3$ structures the Fe-O bond interactions were displaced to -3.5 and -7 eV range and the band-gap was calculated as 1.99 and 2.86 eV, respectively. The $FeSiO_3$ structure band gap calculated was not usual for perovskites. Thus, this material is a great alternative to electronic devices and photocatalysis processes because of the wavelength 623.04 nm located inside the visible ultraviolet. However, in the $FeZrO_3$ model, the Fe-O bond interactions were extended between -2 and -7 eV and the band-gap was calculated as 3.14 eV.

Table 3 Theoretical Results of the Mulliken Population Analysis for ($\alpha + \beta$) atomic charge net (in |e|) and ($\alpha - \beta$) spin net (in |e|) performed on $FeBO_3$ (B = Ti, Si, Sn, Zr) materials.

| Models | ($\alpha + \beta$) | | | ($\alpha - \beta$) | | |
	Fe	B	O	Fe	B	O
$FeTiO_3$	0.840	2.080	-0.970	3.810	0.011	0.061
$FeSiO_3$	0.765	2.245	-1.003	3.780	0.003	0.073
$FeSnO_3$	0.812	2.652	-1.155	3.825	-0.018	0.064
$FeZrO_3$	0.906	2.962	-1.289	3.805	0.030	0.055

The theoretical results obtained from Mulliken Population Analysis applied to atomic charge and spin state (Table 3) were used for analyzing the electronic density distribution in the different materials. The ($\alpha + \beta$) notation used to analyze charge net was related to electronic total contribution to atomic charge; whereas, ($\alpha - \beta$) notation was used to represent the unpaired electronic spins inside the molecular structure. Due to the dependence of the Mulliken Population Analysis in relation to atomic basis set, the discussion about atomic charge will be carried out through a qualitative viewpoint and the $FeTiO_3$ material atomic charges will be used as reference. In general, the Fe atomic charge is barely modified by B = Ti, Si, Sn, Zr cation; whereas, B and O atomic charges increase when B cation is replaced in the order: Ti< Si < Sn <Zr. This charge distribution indicates an increase in the ionic bond to $FeTiO_3$, $FeSiO_3$, $FeSnO_3$ and $FeZrO_3$ materials, respectively; showing evidence to increase the charge separation among atoms and, consequently, increase in the spontaneous polarization, which is directly influenced by the ferroelectric property.

Regarding the electronic spin (Table 3), it was observed that only the Fe atoms had unpaired spins; whereas, for B and O atoms the spins were paired, as expected. Spin values calculated for Fe atoms were in agreement with 3d^6 electronic

configuration and these values were not modified by B cation. This result showed that the replacement of the B cation in the ilmenite structure changed the atomic charge distribution but

the spin moment from unpaired spins related to Fe atom was not modified.

Table 4 Theoretical results for overlap population (in m|e|) of the M-O bonds in the $FeBO_3$ (B = Ti, Si, Sn, Zr) structures.

Models	Overlap Populations M-O							
	$\alpha + \beta$				$\alpha - \beta$			
	Fe-O$_{ax.}$	Fe-O$_{eq.}$	B-O$_{ax.}$	B-O$_{eq.}$	Fe-O$_{ax.}$	Fe-O$_{eq.}$	B-O$_{ax.}$	B-O$_{eq.}$
$FeTiO_3$	18	1	19	61	-25	-29	0	2
$FeSiO_3$	-11	-17	145	194	-22	-28	0	1
$FeSnO_3$	-3	10	71	146	-19	-24	2	3
$FeZrO_3$	12	37	30	40	-22	-22	1	1

Therefore, it was expected that ferroelectric property changed; however, no alterations were expected in the magnetic property in relation to $FeTiO_3$ material. The negative spin value calculated to Sn atom was expected because the pseudopotential basis set causes this kind of distortion.[61-63]

Overlap population results were obtained for Fe-O and B-O (B = Ti, Si, Sn, Zr) bonds in axial and equatorial planes (Table 4). Regarding the overlap population for $(\alpha + \beta)$ charge net, Fe-O bonds were predominantly ionic, except for the Fe-O$_{eq}$ bond in the $FeZrO_3$ material, which had a more evidenced covalent bond character. B-O bonds were predominantly covalent in all structures, in particular, the B-O bonds for $FeSiO_3$ and $FeSnO_3$ materials were the most overlapped; whereas, only B-O$_{ax}$ bond in the $FeTiO_3$ structure showed ionic overlap. It was observed that every Si-O bonds had bonding character and was highly overlapped; in contrast, Fe-O bonds in the $FeSiO_3$ material had anti bonding character. Such calculated results of the $FeSiO_3$ structure were in agreement with Bulk-Modulus because the great bonding character located among Si-O bonds, was opposite to the antibonding character located among Fe-O bonds, favouring a Bulk-Modulus result less than that expected from relative density (ρ). All overlap population results can be interpreted as influenced by the highest electronegativity of Si and Sn metals and showed the effect on the electronegativity of the stability of the ilmenite structure.[64]

In relation to $(\alpha - \beta)$ spin net overlap population, every Fe-O bonds showed antibonding character because of unpaired spins at $3d^6$ configuration for Fe atoms. The B-O bonds were calculated as approximately null confirming the total pairing of the electrons in these bonds.

[Insert Figure 4]

Another path to visualize the electronic density distribution in the $FeBO_3$ structures is through the analysis of charge density maps. It is important to comment that these results were obtained from optimized wave function of the structures and, the final result was related to all electrons electronic density. Figure 4 shows electron density maps for $FeBO_3$ (B = Ti, Si, Sn, Zr) materials. The crystallographic plane chosen was a vertical plane in the [001] direction containing Fe, B and O atoms. This choice was important because the electronic share among octahedral clusters was shown to make an electronic path, mainly used for carrying spins and, consequently, enabling the use of $FeBO_3$ materials in the spintronic. Then, the $FeTiO_3$, $FeSiO_3$, $FeSnO_3$ and $FeZrO_3$ structures calculated charge density maps clearly showed electronic paths (Fig. 4 in green colour) located among O-Fe-O-B-O (B = Ti, Si, Zr) bonds in the [001] direction. Therefore, these electronic paths were the bonding paths to share electrons among FeO_6 and BO_6 octahedral clusters and, which mainly carry spins through the crystalline structure. For $FeSnO_3$ the bonding paths were not completely calculated because the Sn atom was described from the pseudopotential basis set.

Conclusions

From theoretical results obtained through DFT/B3LYP theory applied to the ilmenite structure of $FeBO_3$ (B = Ti, Si, Sn, Zr) materials, it was observed that lattice parameters and bulk-modulus for $FeTiO_3$ material were calculated with good agreement with the experimental results. Regarding structural properties, changes were observed at the unit cell caused by B-O bond distance. Elastic properties calculated from bulk-modulus revealed the influence of relative density and coordination number in the ilmenite structure. In particular, the $FeSnO_3$ presented a negative value for bulk-modulus due to high packing density determining a thermodynamic instability under equilibrium conditions. Electronic properties of $FeBO_3$ materials were modified due to the occupation of the B site by the atom. DOS results showed that the Fe-O bonding interaction and band-gap results were influenced by different occupied energy levels of B (B = Ti, Si, Sn, Zr) cations in different materials. Mulliken Population Analysis showed satisfactory results for these models demonstrating the magnetic character of the iron atoms in $3d^6$ configuration. Overlap theoretical results indicated that the electronegativity of metals occupying the B site affected the ilmenite structure stability in agreement with other studies in the literature. Electron density maps showed the formation of a charge corridor in [001] direction due to the intermetallic connection of FeO_6 and BO_6 clusters. The summation of these theoretical results demonstrated that current computational simulations are very useful to rationalize the effect of metals occupying ilmenite structure B-site on the structural, electronic and elastic properties of such materials.

Acknowledgements

Notes and references

^{a}Department of Chemistry, State University of Ponta Grossa, Av. Gen. Carlos Cavalcanti, 4748, Zip-Code: 84030-900, Ponta Grossa, Brazil. E-mail: srlazaro@uepg.br; Fax: +55 4232203042.

1. W. Xiao, X.-G. Lu, X.-L. Zou, X.-M. Wei and W.-Z. Ding, *Trans. Nonferrous Met. Soc. China*, 2013, **23**, 2439-2445.
2. Y. J. Kim, B. Gao, S. Y. Han, M. H. Jung, A. K. Chakraborty, T. Ko, C. Lee and W. I. Lee, *J. Phys. Chem. C*, 2009, **113**, 19179-19184.
3. S. Ohara, K. Sato, Z. Tan, H. Shimoda, M. Ueda and T. Fukui, *J. Alloys Compd.*, 2010, **504**, L17-L19.
4. T. Tao, A. M. Glushenkov, H. Liu, Z. Liu, X. J. Dai, H. Chen, S. P. Ringer and Y. Chen, *J. Phys. Chem. C*, 2011, **115**, 17297-17302.

RSC Advances Accepted Manuscript

5. A. T. Raghavender, N. Hoa Hong, K. Joon Lee, M.-H. Jung, Z. Skoko, M. Vasilevskiy, M. F. Cerqueira and A. P. Samantilleke, *J. Magn. Magn. Mater.*, 2013, **331**, 129-132.

6. T. Yamanaka, Y. Komatsu and H. Nomori, *Phys Chem Minerals*, 2007, **34**, 307-318.

7. E. J. Tronche, J. Van Kan Parker, J. Vries, Y. Wang, T. Sanehira, J. Li, B. Chen, L. Gao, S. Klemme, McCammon and W. van Westrenen, *Am. Mineral.*, 2010, **95**, 1708-1716.

8. T. Fujii, M. Yamashita, S. Fujimori, Y. Saitoh, T. Nakamura, K. Kobayashi and J. Takada, *J. Magn. Magn. Mater.*, 2007, **310**, e555-e557.

9. S. W. Chen, M. J. Huang, P. A. Lin, H. T. Jeng, J. M. Lee, S. C. Haw, S. A. Chen, H. J. Lin, K. T. Lu, D. P. Chen, S. X. Dou, X. L. Wang and J. M. Chen, *Appl. Phys. Lett.*, 2013, **102**, 042107.

10. K. Leinenweber, W. Utsumi, Y. Tsuchida, T. Yagi and K. Kurita, *Phys Chem Minerals*, 1991, **18**, 244-250.

11. X. Wu, G. Steinle-Neumann, O. Narygina, I. Kantor, C. McCammon, S. Pascarelli, G. Aquilanti, V. Prakapenka and L. Dubrovinsky, *Phys. Rev. B: Condens. Matter Mater. Phys.*, 2009, **79**, 094106.

12. T. Varga, A. Kumar, E. Vlahos, S. Denev, M. Park, S. Hong, T. Sanehira, Y. Wang, C. J. Fennie, S. K. Streiffer, X. Ke, P. Schiffer, V. Gopalan and J. F. Mitchell, *Phys. Rev. Lett.*, 2009, **103**, 047601.

13. C. J. Fennie, *Phys. Rev. Lett.*, 2008, **100**, 167203.

14. N.-N. Ge, C.-M. Liu, Y. Cheng, X.-R. Chen and G.-F. Ji, *Phys. B (Amsterdam, Neth.)*, 2011, **406**, 742-748.

15. A. Stashans, L. Eras and G. Chamba, *Phys Chem Minerals*, 2010, **37**, 191-199.

16. D. Nakatsuka, T. Yoshino, J. Kano, H. Hashimoto, M. Nakanishi, J. Takada and T. Fujii, *J. Solid State Chem.*, 2013, **198**, 520-524.

17. T. Okada, T. Narita, T. Nagai and T. Yamanaka, *Am. Mineral.*, 2008, **93**, 39-47.

18. N. A. Benedek and C. J. Fennie, *J. Phys. Chem. C*, 2013, **117**, 13339-13349.

19. J. Y. Son, G. Lee, M.-H. Jo, H. Kim, H. M. Jang and Y.-H. Shin, *J. Am. Chem. Soc.*, 2009, **131**, 8386-8387.

20. Y. Inaguma, M. Yoshida and T. Katsumata, *J. Am. Chem. Soc.*, 2008, **130**, 6704-6705.

21. A. Aimi, T. Katsumata, D. Mori, D. Fu, M. Itoh, T. r. Kyômen, K.-i. Hiraki, T. Takahashi and Y. Inaguma, *Inorg. Chem.*, 2011, **50**, 6392-6398.

22. Y. Yan, Y. Li, Z. Fang, G. Wang and Y. Ma, *High Pressure Res.*, 2010, **30**, 292-300.

23. A. Stashans, K. Rivera and H. P. Pinto, *Phys. B. (Amsterdam, Neth)*, 2012, **407**, 2037-2043.

24. W.-L. Zhu, X.-Y. Chen, Y.-J. Zhao and T.-S. Lai, *Int. J. Mod. Phys. B*, 2014, **28**, 1450224.

25. S. C. Middleburgh, I. Karatchevtseva, B. J. Kennedy, P. A. Burr, Z. Zhang, E. Reynolds, R. W. Grimes and G. R. Lumpkin, *J. Mater. Chem. A.*, 2014, **2**, 15883-15888.

26. F. Litimein, R. Khenata, A. Bouhemadou, Y. Al-Douri and S. B. Omran, *Mol. Phys.*, 2011, **110**, 121-128.

27. A. B. Alexei and Y. Wei, *J. Phys.: Condens. Matter*, 2014, **26**, 163201.

28. L. Guo, S. Zhang, W. Feng, G. Hu and W. Li, *J. Alloys Compd.*, 2013, **579**, 583-593.

29. B. S. Omran, B. Amin, G. Murtaza, R. Khanata and R. Ali, *Int. J. Mod. Phys. B*, 2013, **27**, 1350170.

30. Y. Liu, Y. Jiang, R. Zhou and J. Feng, *J. Alloys Compd.*, 2014, **582**, 500-504.

31. S. Gong, P. Chen and B. G. Liu, *J. Magn. Magn. Mater.*, 2014, **349**, 74-79.

32. O. Sahnoun, H. Bouhani-Benziane, M. Sahnoun, M. Driz and C. Daul, *Comput. Mater. Sci.*, 2013, **77**, 316-321.

33. J. Hafner, C. Wolverton and G. Ceder, *MRS Bull.*, 2006, **31**, 659-668.

34. Z.-y. Chen and J.-l. Yang, *Front. Phys. China*, 2006, **1**, 339-343.

35. B. G. Janesko, T. M. Henderson and G. E. Scuseria, *Phys. Chem. Chem. Phys.*, 2009, **11**, 443-454.

36. F. Corà, M. Alfredsson, G. Mallia, D. Middlemiss, W. Mackrodt, R. Dovesi and R. Orlando, in *Principles and Applications of Density Functional Theory in Inorganic Chemistry II*, Springer Berlin Heidelberg, Editon edn., 2004, vol. 113, pp. 171-232.

37. J. Muscat, A. Wander and N. M. Harrison, *Chem. Phys. Lett.*, 2001, **342**, 397-401.

38. B. A. Wechsler and C. T. Prewitt, *Am. Mineral.*, 1984, **69**, 176-185.

39. A. D. Becke, *J. Chem. Phys.*, 1993, **98**, 5648-5652.

40. A. D. Becke, *Phys. Rev. A: At., Mol., Opt. Phys.*, 1988, **38**, 3098-3100.

41. C. Lee, W. Yang and R. G. Parr, *Phys. Rev. B: Condens. Matter Mater. Phys.*, 1988, **37**, 785-789.

42. R. Dovesi, R. Orlando, B. Civalleri, C. Roetti, V. R. Saunders and C. M. Zicovich-Wilson, *Z. Kristallogr.—New Cryst. Struct.*, 2005, **220**, 571-573.

43. M. F. Peintinger, D. V. Oliveira and T. Bredow, *J. Comput. Chem.*, 2013, **34**, 451-459.

44. M. Causà, R. Dovesi and C. Roetti, *Phys. Rev. B: Condens. Matter Mater. Phys.*, 1991, **43**, 11937-11943.

45. P. Durand and J.-C. Barthelat, *Theoret. Chim. Acta*, 1975, **38**, 283-302.

46. H. J. Monkhorst and J. D. Pack, *Phys. Rev. B: Condens. Matter Mater. Phys.*, 1976, **13**, 5188-5192.

47. N. C. Wilson and S. P. Russo, *Phys. Rev. B: Condens. Matter Mater. Phys.*, 2011, **84**, 075310.

48. R. Dovesi, V. R. Saunders, C. Roetti, R. Orlando, C. M. Zicovich-Wilson, F. Pascale, B. Civalleri, K. Doll, N. M. Harrison, I. J. Bush, P. D'Arco and M. Llunell, *CRYSTAL09 User's Manual*, University of Torino, Torino, 2009.

49. N. C. Wilson, J. Muscat, D. Mkhonto, P. E. Ngoepe and N. M. Harrison, *Phys. Rev. B: Condens. Matter Mater. Phys.*, 2005, **71**, 075202.

50. J. Klafter and J. Jortner, *J. Chem. Phys.*, 1978, **68**, 1513-1522.

51. M. S. Pierce, J. E. Davies, J. J. Turner, K. Chesnel, E. E. Fullerton, J. Nam, R. Hailstone, R. Kevan, J. B. Kortright, K. Liu, L. B. Sorensen, B. R. York and O. Hellwig, *Phys. Rev. B: Condens. Matter Mater. Phys.*, 2013, **87**, 184428.

52. X.-P. Hu, D.-W. Duan, K. Zhang, Y.-C. Zhang, S.-Q. Chu, J. Zhang, Y.-N. Xie, D. Guo and J.-L. Cao, *Ferroelectrics*, 2013, **453**, 149-155.

53. F. D. Murnaghan, *Proc. Natl. Acad. Sci. U. S. A.*, 1944, **30**, 244-247.

54. C. L. Muhlstein and S. B. Brown, *Mechanical Properties of Structural Films*, ASTM International, New York, 2001.

55. A. R. West, *Solid State Chemistry and Its Applications*, 2 edn., Wiley, Chichester, 1985.

56. Y. A. Wang and R. S. Lakes, *J. Compos. Mater.*, 2005, **39**, 1645-1657.

57. P. D. S. Jr, J. M. Henriques, C. A. Barboza, E. L. Albuquerque, V. N. Freire and E. W. S. Caetano, *J. Phys.: Condens. Matter*, 2010, **22**, 435801.

58. J. M. Henriques, E. W. S. Caetano, V. N. Freire, J. A. P. d. Costa and E. L. Albuquerque, *J. Phys.: Condens. Matter*, 2007, **19**, 106214.

59. X. Tang and K.-a. Hu, *J Mater Sci*, 2006, **41**, 8025-8028.

60. D. S. Ginley and M. A. Butler, *J. Appl. Phys. (Melville, NY, U. S.)*, 1977, **48**, 2019-2021.

61. R. A. Evarestov, in *Quantum Chemistry of Solids*, Springer, Heidelberg, Editon edn., 2007, vol. 153, pp. 281-326.

62. J. J. Philips, M. A. Hudspeth, P. M. Browne Jr and J. E. Peralta, *Chem. Phys. Lett.*, 2010, **495**, 146-150.

63. E. Ruiz, J. Cirera and S. Alvarez, *Coord. Chem. Rev.*, 2005, **249**, 2649-2660.

64. X. Liu, R. Hong and C. Tian, *J Mater Sci: Mater Electron*, 2009, **20**, 323-327.

RSC Advances Accepted Manuscript

Journal Name

ARTICLE

Figures and Captions
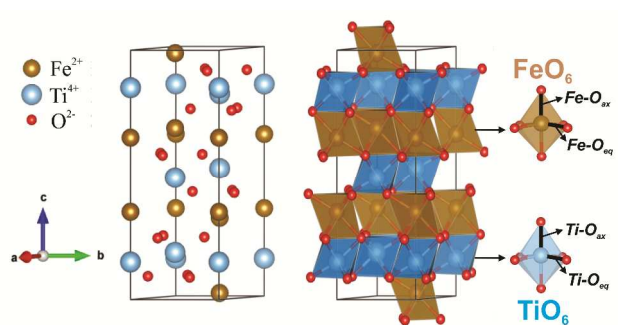
Figure 1. $FeTiO_3$ material unit cell. The yellow, blue and red balls represent Fe, Ti and O atoms, respectively. The orange and blue octahedral represent the FeO_6 and TiO_6 clusters, respectively.
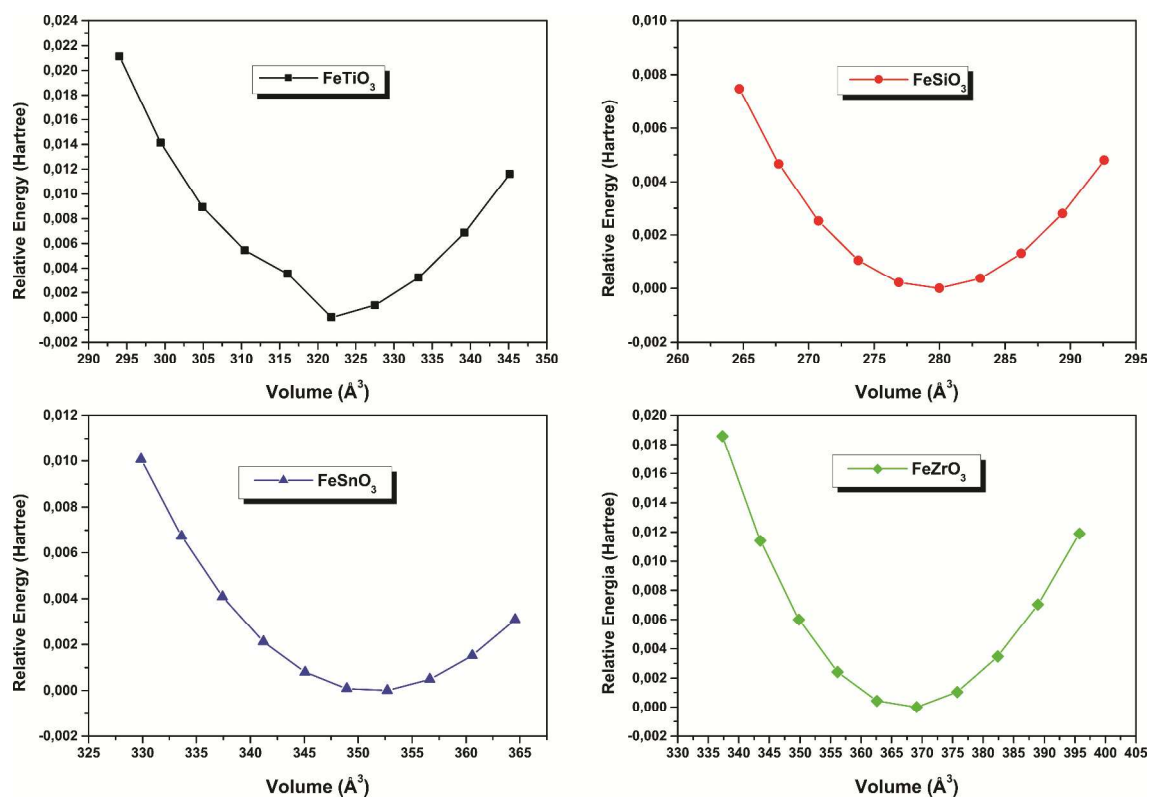
Figure 2. Energy vs Volume (EOS) theoretical curves for $FeBO_3$ (B = Ti, Si, Sn, Zr) materials.
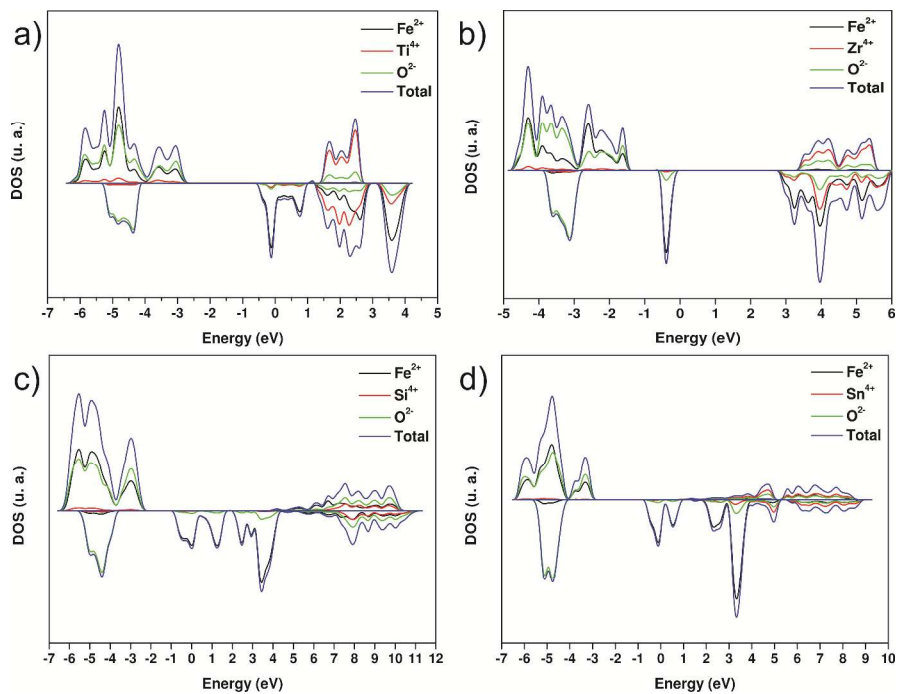
Figure 3. Density of States (DOS) for (a) FeTiO₃, (b) FeSiO₃, (c) FeSnO₃ and (d) FeZrO₃ materials.
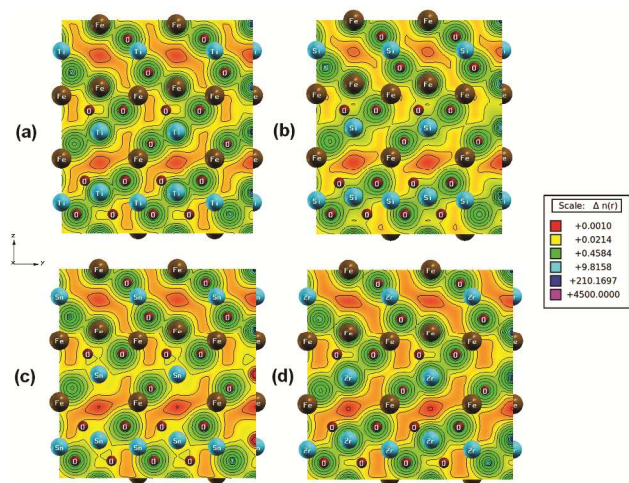
Figure 4. Bonding paths to carry spins obtained from electron density maps: (a) FeTiO$_3$, (b) FeSiO$_3$, (c) FeSnO$_3$ and (d) FeZrO$_3$.

Graphical Abstract

Intermetallic Connection

Bulk-Modulus

[FeO₆]

[BO₆]

Stability Factors

Fe²⁺

B⁴⁺

B = Ti, Si, Sn, Zr
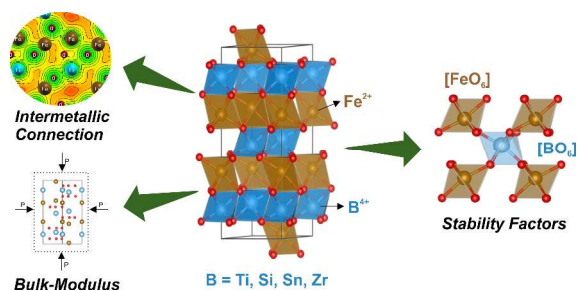
A DFT study to investigate the effects of B-cation replacement on the ilmenite structure structural, electronic and elastic properties is reported.